Intermediate mass excess of dilepton production in heavy ion collisions at relativistic energies

C. Ernst,* S. A. Bass,† M. Belkacem, H. Stöcker, and W. Greiner

Institut für Theoretische Physik, J. W. Goethe-Universität, D-60054 Frankfurt am Main, Germany

(Received 26 January 1998)

Dielectron mass spectra are examined for various nuclear reactions recently measured by the DLS Collaboration. A detailed description is given of all dilepton channels included in the transport model UrQMD 1.0, i.e., Dalitz decays of $\pi^0, \eta, \omega, \eta'$ mesons and of the $\Delta(1232)$ resonance, direct decays of vector mesons and pn bremsstrahlung. The microscopic calculations reproduce data for light systems fairly well, but tend to underestimate the data in pp at high energies and in pd at low energies. These conventional sources, however, cannot explain the recently reported enhancement for nucleus-nucleus collisions in the mass region $0.15 \text{ GeV} \leq M_{e^+e^-} \leq 0.6$ GeV. Chiral scaling and ω meson broadening in the medium are investigated as a source of this mass excess. They also cannot explain the recent DLS data. [S0556-2813(98)01007-3]

PACS number(s): 25.75.−q

I. INTRODUCTION

Dileptons have been proposed in the late 70's as penetrating probes [1] of hot and dense nuclear systems. They are presumably created in all stages of heavy ion reactions by several distinct mechanisms. Once produced, they practically do not interact with the surrounding hadronic matter. Low mass dileptons are of particular interest (see, e.g., [2–7]). They can reveal information of the *hadronic* properties in the reaction zone. Several experiments have focused on low mass lepton pairs: the DLS spectrometer at the BEVALAC [8,9], the CERES and HELIOS detectors at the SPS at CERN [10]. The dilepton spectrometers HADES at SIS at GSI [11] and PHENIX at RHIC in BNL [12] are under construction. The most striking result of the high-energy dilepton programs so far is the observed enhancement in heavy systems at low invariant masses as compared to ''conventional'' hadronic cocktails and models. A dropping mass [13,14] or dissolving spectral function [15,16] of the ρ meson have been offered in attempt to explain these data. Recently, a systematic measurement of dilepton production at BEVALAC energies has been published. Data are available for elementary pp and pd collisions as well as for nucleus-nucleus collisions [8,9].

The aim of the present work is to investigate dilepton production within the microscopic n-body transport model UrQMD. The outline of the paper is as follows: In Sec. II a brief survey of the UrQMD model is given. A more detailed description of the implemented dilepton production mechanisms follows. Section III contains the calculations of the elementary pp and pd dilepton cross sections in comparison to recent DLS measurements. Section IV shows mass spectra for heavier systems. Summary and concluding remarks are given in Sec. V.

II. PRODUCTION OF RESONANCES AND DILEPTONS

A. Hadron production in the UrQMD model

The UrQMD model is based on the quantum molecular dynamics concept [17–19]. The Hamilton's equations of mo-

tion are solved for Gaussian wave packets. The model allows for the production of all established meson and baryon resonances up to about 2 GeV with all corresponding isospin projections and antiparticle states. The collision term describes particle production by resonant excitation channels and, for higher masses, within a string fragmentation scheme. The UrQMD model is designed to cover consistently the whole range of bombarding energies per nucleon from 200 MeV to 200 GeV. For dilepton production at BEVALAC energies, the resonant production of neutral mesons is most important. A detailed description of the model can be found in Refs. [20,21].

The formation of light mesons at low energies is modeled as a multistep process that proceeds via intermediate heavy baryon and meson resonances and their subsequent decay [22]. The resonance parameters (pole masses, widths, and branching ratios) are taken from [23], but large uncertainties of these parameters are used to obtain a consistent fit to cross section data. For example, the production of ω mesons is described in the UrQMD model by the formation and the decay of the $N^\star(1900)$ resonance. It decays to 35% into $N\pi$ and to 55% into $N\omega$. As suggested in Ref. [24], the η production proceeds not only via $N^\star(1535)$, but invokes also nucleon resonances with masses 1650, 1700, 1710, and 2080 MeV. A full list of the UrQMD resonance parameters is published in Ref. [20].

For the resonance cross sections in baryon-baryon, meson-baryon, and meson-meson collisions, conventional Breit-Wigner parametrizations are used with mass dependent widths. At higher energies the resonant particle production does no longer predict the observed cross sections. There, the string picture, described in [20], is employed.

Figure 1 shows calculations of exclusive ($pp \rightarrow mpp$) and inclusive ($pp \rightarrow mX$) cross sections for the production of neutral mesons $m = \pi^0, \eta, \rho^0, \omega$ as a function of the excess energies $\epsilon = \sqrt{s} - \sqrt{s_{th}}$. Here $\sqrt{s_{th}}$ is the energy of the production threshold calculated as $\sqrt{s_{th}} = 2m_p + m_m$ with the proton mass m_p and the pole mass of the meson m_m. In the case of ρ^0 mesons we count only those with masses within ± 100 MeV around the pole mass to compare with data. The exclusive η production just above threshold [25] is overestimated by a factor of about two. The arrows along x axis of the

─────────

*Electronic address: ernst@th.physik.uni-frankfurt.de

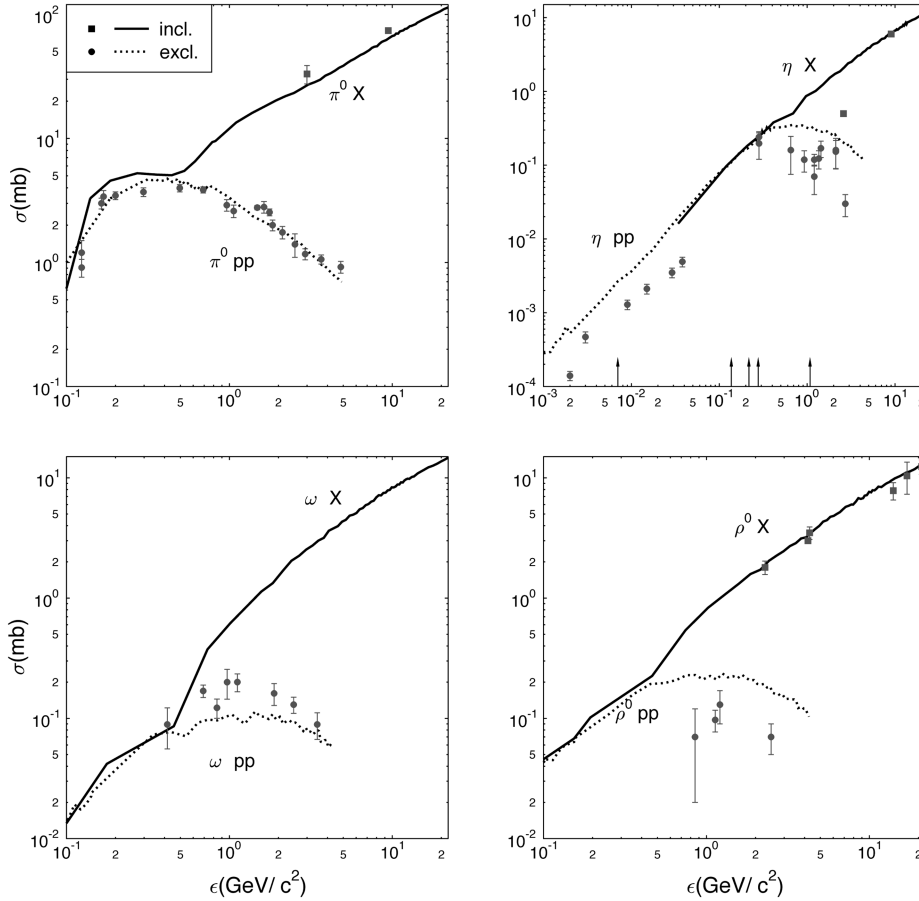†Present address: Department of Physics, Duke University, Durham, NC 27708-0305.

FIG. 1. Cross sections for neutral meson production in pp collisions as a function of the excess energy $\epsilon = \sqrt{s} - \sqrt{s_{\text{th}}}$. Calculations are shown for the exclusive and inclusive production of π^0, η, ω, and ρ^0 mesons in comparison to available data [51,25]. The arrows in the η plot refer to incident energies of $E_{\text{kin}} = 1.27$, 1.65, 1.85, 2.09, and 4.88 GeV, respectively.

upper right panel indicate the incident energies of 1.27 GeV, 1.61 GeV, 1.85 GeV, 2.09 GeV, and 4.88 GeV. Note that above 3.5 GeV the exclusive cross sections become less important because the string channel opens and allows for multiple resonance production. For the present article the relevant $\sqrt{s}$ values are below 4 GeV, where so far no data on the inclusive channels are available.

B. Dilepton radiation in UrQMD

Dileptons can be produced in hadronic decays and collisions. The mechanisms that are expected to dominate in the low-mass region (with invariant dilepton masses below 1 GeV) are the Dalitz decays ($A \to B e^+ e^-$) of neutral mesons $\pi^0, \eta, \eta', \omega$, as well as the Dalitz decay of the $\Delta(1232)$ resonance. Around their pole masses the direct decays ($A \to e^+ e^-$) of the vector mesons ρ^0, ω, and ϕ are expected to dominate the spectrum. These modes are of special interest: the invariant mass of the dilepton equals the vector meson mass in the hot and dense medium. Also included in the present model calculation is the pn bremsstrahlung. It contributes especially at low bombarding energies. In accord with Ref. [3], other sources like Dalitz decays of heavier resonances, pp, πN bremsstrahlung, etc., are neglected for the reactions considered here. Direct dilepton production in binary collisions, e.g. $\pi^+\pi^-, K^+K^- \to e^+ e^-$, or $\pi\rho \to e^+ e^-$, is not evaluated. In the framework of the present model this would correspond to a partial double counting: these reactions are supposedly included as explicit multistep processes (e.g., $\pi\rho \to \phi \to e^+ e^-$). This also holds for the

Dalitz decay of the $a_1 \to \pi\rho \to \pi e^+ e^-$. At higher bombarding energies, however, direct processes like $\pi\rho \to \pi e^+ e^-$ might significantly contribute to the dilepton yield [26].

1. Dalitz decays of mesons

Decays of the type $A \to B e^+ e^-$ are not real multibody decays (for which usually the name Dalitz is used), but can be reduced to a decay into B plus a virtual photon (with an invariant mass M) and subsequent conversion of the latter. Thus the matrix element factorizes [27,28]

$$|\mathcal{M}|^2 = |\mathcal{M}(A \to B\gamma^*)|^2 \frac{1}{M^4} |\mathcal{M}(\gamma^* \to e^+ e^-)|^2. \quad (1)$$

This reflects in the differential decay rate, which can be written as a product of the conversion rate of the virtual gamma [29] and the decay width $\Gamma_{A \to B\gamma^*}$ of A into a massive photon:

$$\frac{d\Gamma_{A \to B e^+ e^-}}{dM} = \frac{2\alpha}{3\pi M} \sqrt{1 - \frac{4m_e^2}{M^2}} \left(1 + \frac{2m_e^2}{M^2}\right) \Gamma_{A \to B\gamma^*}, \quad (2)$$

where m_e is the lepton mass. If one assumes that A decays isotropically in its rest frame, the $A \to B\gamma^*$ width is given by

$$\Gamma_{A\to B\gamma*}=\frac{|\vec{p}_{cm}|}{8\pi m_A^2}|\mathcal{M}_{A\to B\gamma*}|^2. \tag{3}$$

Here $|\vec{p}_{cm}|$ is the decay momentum

$$|\vec{p}_{cm}|=\frac{\lambda^{1/2}(m_A^2,m_B^2,M^2)}{2m_A} \tag{4}$$

with the kinematic function $\lambda(x^2,y^2,z^2)=(x^2-(y+z)^2)(x^2-(y-z)^2)$.

A remaining difficulty resides in the calculation of the matrix element of the $A\to B\gamma*$ decay. The meson decays considered here are either of the type (a) pseudoscalar (π^0,η,η') into a vector particle (γ) plus a virtual photon or (b) vector meson (ω) into a pseudoscalar meson plus a virtual photon. In both cases one gets [30]

$$|\mathcal{M}_{A\to B\gamma*}|^2=\tfrac{1}{2}|f_{AB}(M^2)|^2\lambda(m_A^2,m_B^2,M^2). \tag{5}$$

The form factor $f_{AB}(M^2)$ is introduced to account for the strong interaction part of the vertex. It is common to normalize to the decay width into real photons [30] by dividing

$$\Gamma_{A\to B\gamma}=\frac{(m_A^2-m_B^2)^3}{32\pi m_A^3}|f_{AB}(0)|^2, \tag{6}$$

which re-expresses the form factors to $F_{AB}(M^2)=f_{AB}(M^2)/f_{AB}(0)$.

The form factors can be obtained from the vector meson dominance model (VMD). In the present calculations the following parametrizations are employed [28,6]

$$F_{\pi^0}(M^2)=1+b_{\pi^0}M^2,$$

$$F_\eta(M^2)=\left(1-\frac{M^2}{\Lambda_\eta^2}\right)^{-1},$$

$$|F_\omega(M^2)|^2=\frac{\Lambda_\omega^2(\Lambda_\omega^2+\gamma_\omega^2)}{(\Lambda_\omega^2-M^2)^2+\Lambda_\omega^2\gamma_\omega^2},$$

$$|F_{\eta'}(M^2)|^2=\frac{\Lambda_{\eta'}^2(\Lambda_{\eta'}^2+\gamma_{\eta'}^2)}{(\Lambda_{\eta'}^2-M^2)^2+\Lambda_{\eta'}^2\gamma_{\eta'}^2} \tag{7}$$

with $b_{\pi^0}=5.5$ GeV^{-2}, $\Lambda_\eta=0.72$ GeV, $\Lambda_\omega=0.65$ GeV, $\gamma_\omega=0.04$ GeV, $\Lambda_{\eta'}=0.76$ GeV, and $\gamma_\eta'=0.10$ GeV.

2. Delta Dalitz decay

The situation is more complicated for the Dalitz decay of the $\Delta(1232)$ resonance. To complete Eqs. (2) and (3), the matrix element for the process $\Delta\to N\gamma*$ has to be calculated. The corresponding interaction vertex has been analyzed by Jones and Scadron [31] in the form

$$\mathcal{L}_{int}=e\bar{\Psi}_\beta\Gamma^{\beta\mu}A_\mu\psi+\text{H.c.}, \tag{8}$$

where ψ, Ψ_β, and A_μ represent the fields of the nucleon, of the delta and of the photon, respectively. The dominant magnetic dipole transition yields the vertex function

$$\Gamma^{\beta\mu}=G_M(M^2)\frac{-3(m_\Delta+m_N)}{2m_N[(m_\Delta+m_N)^2-M^2]}$$
$$\times(-m_\Delta\chi_1^{\beta\mu}\gamma_5+\chi_2^{\beta\mu}\gamma_5+\tfrac{1}{2}\chi_3^{\beta\mu}\gamma_5). \tag{9}$$

The choice of the χ bears some freedom if only current conservation is ensured ($q_\beta\Gamma^{\beta\mu}=0$). Following Ref. [31], one may write

$$\chi_1^{\beta\mu}=(q^\beta\gamma^\mu-q\cdot\gamma g^{\beta\mu}),$$

$$\chi_2^{\beta\mu}=(q^\beta P^\mu-q\cdot P g^{\beta\mu}), \tag{10}$$

$$\chi_3^{\mu\beta}=(q^\beta q^\mu-q^2 g^{\beta\mu}),$$

with $P=1/2(p_\Delta+p_N)$ and $q=p_\Delta-p_N$. G_M in Eq. (9) stands for the magnetic dipole form factor. It can be fixed at $M=0$ to the decay into a real photon, yielding $G_M(0)=3.0$. The M-dependence of the overall form factor is subject to speculation: the timelike electromagnetic form factors for baryons are unknown in the kinematic region of interest. In the present calculation of the Δ Dalitz contribution all VMD-type form factors are omitted. This provides a lower limit to his source in the region of the vector meson poles.

Using Eqs. (8) and (9), we can express the matrix element via

$$\hat{\mathcal{M}}_i=e\bar{u}_\beta(p_\Delta,s_\Delta)\chi_i^{\beta\mu}\gamma_5\epsilon_\mu(p_\gamma,s_\gamma)u(p_N,s_N). \tag{11}$$

The matrix element may be written as a linear combination of the $\hat{\mathcal{M}}_i$ and $\hat{\mathcal{M}}_j^*$:

$$|\mathcal{M}|^2=e^2G_M^2\frac{9(m_\Delta+m_N)^2}{4m_N^2[(m_\Delta+m_N)^2-M^2]^2}$$
$$\times\sum_{i,j=1}^3 c_i\hat{\mathcal{M}}_i c_j\hat{\mathcal{M}}_j^*, \tag{12}$$

where $c_1=-m_\Delta$, $c_2=1$, and $c_3=1/2$. The appearing traces have been calculated using the *Mathematica* package HIP [32]. One then obtains:

$$\sum_{i,j=1}^3 c_i\hat{\mathcal{M}}_i c_j\hat{\mathcal{M}}_j^*=\frac{1}{9}((m_\Delta-m_N)^2-M^2)(7m_\Delta^4+14m_\Delta^2M^2$$
$$+3M^4+8m_\Delta^3 m_N+2m_\Delta^2 m_N^2$$
$$+6M^2 m_N^2+3m_N^4). \tag{13}$$

After substituting Eqs. (12) and (13) into Eq. (3), one gets the Δ Dalitz decay width.

Figure 2 shows the differential mass distributions of the Dalitz decay probabilities as implemented into the UrQMD model. While the very low masses are dominated by π^0 and η decays, the ω and η' decays are more important at higher masses. The contributions of the Δ decays are also shown for different masses of the $\Delta(1232)$. Heavy Δ's naturally contribute more to the probabilities than lighter ones. In calculating the dilepton spectrum, these probabilities are multiplied with the yields of the corresponding particle species. At low energies the dominant $\pi N\Delta$ system [18] can push the Δ
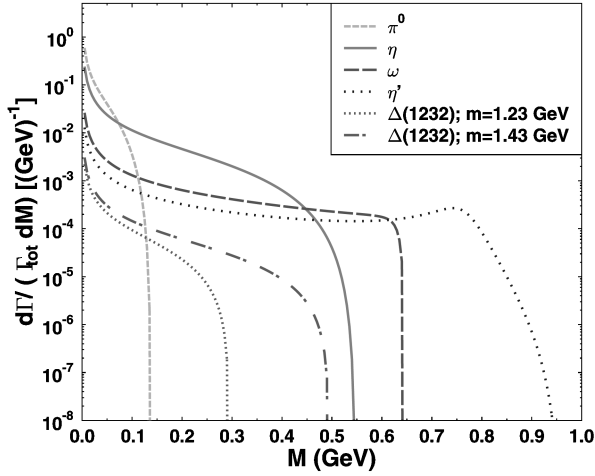
FIG. 2. Differential probability distributions for Dalitz decays. The mass-differential branching ratios for decays of π^0 (dashed), η (solid), ω (long-dashed), and η' (dotted) mesons can be seen. Also shown is the parametrization for Dalitz decays of the $\Delta(1232)$ resonances at pole mass (dotted) and of a heavy $\Delta(1232)$ with mass $m_\Delta = 1.432$ GeV (dash-dotted).

contributions over those of the heavy mesons. On the other hand, the small yield of the η' will make it invisible, due to the tremendous background of other sources in the relevant mass region.

3. Direct decays of vector mesons

The decay width of the electromagnetic two-body decays of the vector mesons are assumed (similar to Ref. [6]) to be of the form

$$\Gamma_{V \to e^+ e^-}(M) = \frac{c_V}{M^3} \sqrt{1 - \frac{4m_e^2}{M^2}} \left(1 + \frac{2m_e^2}{M^2}\right) \Theta(M - 2m_e). \tag{14}$$

The constants c_V are fitted to yield the vacuum widths given in Ref. [23] at the resonance poles. One obtains $c_\rho = 3.079 \times 10^{-6}$ GeV^4, $c_\omega = 0.287 \times 10^{-6}$ GeV^4, and $c_\phi = 1.450 \times 10^{-6}$ GeV^4.

It is assumed that vector mesons can radiate off dileptons continuously [33]. The dilepton mass distribution is given by the time-integral over the mass distributions of mesons plus an additional term which accounts for the decays after some typical freeze-out time t_f (the last term can be dropped if $t_f \to \infty$)

$$\frac{dN_{ee}}{dM} = \int_0^{t_f} dt \frac{dN_V(t)}{dM} \cdot \Gamma_{V \to ee}(M) + \frac{dN_V(t_f)}{dM} \cdot \frac{\Gamma_{V \to ee}(M)}{\Gamma_{V,\text{tot}}(t_f)}. \tag{15}$$

If absorption is negligible, this approach is equivalent to the method of adding one dilepton (with appropriate normalization) at each decay vertex. However, this "shining" method gives a better sampling of the density probed by the hadron and thus a better statistics for density dependent spectral functions. In addition, there is generally a complicated time dependence of the total hadron width $\Gamma_{\text{tot}}(t, \vec{r})$, caused by the in-medium modifications of the quasiparticle widths. The ap-

proach Eq. (15) has the advantage to be explicitly independent of the in-medium width, as long as t_f is reasonably high, so that the total width takes on its vacuum properties.

4. Incoherent bremsstrahlung

In the soft photon approximation (SPA) the cross section for real photons with four-momentum q^μ in collisions $a + b \to X$ can be expressed as

$$q_0 \frac{d\sigma_{ab}^{\gamma X}}{d^3 q} = \frac{\alpha}{4\pi^2} |\epsilon \cdot J|^2 d\sigma_{ab}^X. \tag{16}$$

$d\sigma_{ab}^X$ denotes the differential cross section of the (strong) ab interaction without any photon in the final state. ϵ is the polarization vector of the photon. The current J^μ is given by

$$J^\mu(q) = -Q_a \frac{p_a^\mu}{p_a \cdot q} - Q_b \frac{p_b^\mu}{p_b \cdot q} + \sum_{i=1}^{X} Q_i \frac{p_i^\mu}{p_i \cdot q}, \tag{17}$$

where the Q's and p's denote the charges and momenta of the corresponding particles.

The SPA is justified only for $M, q_0 \to 0$. To extrapolate to the case of hard and massive virtual photons, a phase space correction can be applied by multiplying the cross section with the ratio of the phase space integrals with/without a virtual photon [34]. Similarly to Eq. (2) one gets

$$\frac{d\sigma_{ab}^{e^+ e^- X}}{d^3 q dM} = \frac{\alpha^2}{6\pi^3} \sqrt{1 - \frac{4m_e^2}{M^2}} \left(1 + \frac{2m_e^2}{M^2}\right)$$
$$\times |\epsilon \cdot J|^2 \frac{R_n(\bar{s})}{R_n(s)} \frac{d\sigma_{ab}^X}{q_0 M}. \tag{18}$$

Here R_n is defined as

$$R_n(s) = \int d\Phi_n(s, p_1 \ldots p_n), \tag{19}$$

where $d\Phi_n$ is the volume element of the n-dimensional Lorentz invariant phase space and $\bar{s}$ is the squared effective energy of the system after the emission of the γ^*,

$$\bar{s} = s + M^2 - 2\sqrt{s} q_0. \tag{20}$$

The correction factor for two outgoing particles reads

$$\frac{R_2(\bar{s}, m_a^2, m_b^2)}{R_2(s, m_a^2, m_b^2)} = \frac{\lambda^{1/2}(\bar{s}, m_a^2, m_b^2)}{\lambda^{1/2}(s, m_a^2, m_b^2)} \frac{s}{\bar{s}}. \tag{21}$$

Equation (18) is a general expression for the bremsstrahlung dilepton production in the SPA. In the case of proton-neutron bremsstrahlung ($pn \to p'n'\gamma^*$), the current is given by $J^\mu = p_{p'}^\mu / q \cdot p_{p'} - p_p^\mu / q \cdot p_p$. As a result we have

$$|\epsilon \cdot J|^2 = \frac{-t}{q_0^2 m_p^2}, \tag{22}$$

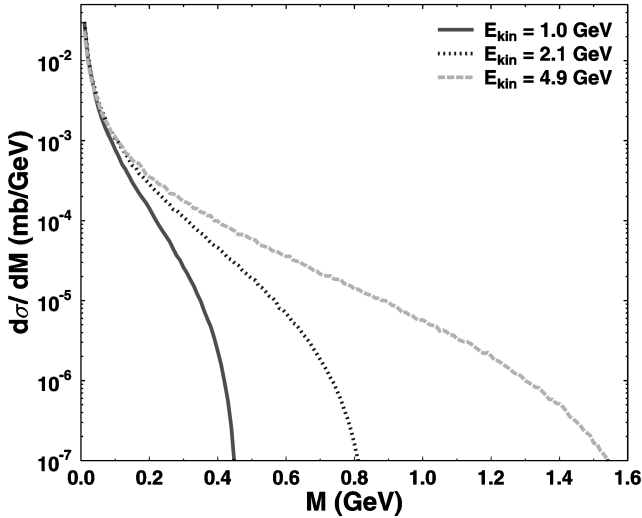with the Mandelstam variable $t = (p_p - p_{p'})^2$. Then Eq. (18) takes the form

FIG. 3. Differential cross section for the production of a bremsstrahlungs pair in elastic pn collisions for beam kinetic energies $E_{kin} = 1.04$ (solid), 2.09 (dotted), and 4.88 GeV (dash-dotted).

$$\frac{d\sigma_{pn}^{pne^+e^-}}{d^3qdM} = \frac{\alpha^2}{6\pi^3}\sqrt{1-\frac{4m_e^2}{M^2}}\left(1+\frac{2m_e^2}{M^2}\right)\frac{\bar{\sigma}}{q_0^3M}\frac{R_2(\bar{s})}{R_2(s)}.$$ (23)

Here $\bar{\sigma}$ is the momentum-transfer weighted pn elastic cross section

$$\bar{\sigma} = \int_{-(s-4m_p^2)}^{0}\left(\frac{-t}{m_p^2}\right)\frac{d\sigma}{dt}dt.$$ (24)

A proper parametrization of $\bar{\sigma}$ is rather important [35]. A systematic overestimation of the differential bremsstrahlung production results if the asymmetry of the momentum-transfer weighted cross section is not included. In the present work a parametrization similar to that of Ref. [35] is used. It consists of a symmetric low-energy part and an asymmetric high-energy component.

Figure 3 shows the cross section for $pn \rightarrow pn + e^+e^-$ bremsstrahlung at different bombarding energies. Note that at low masses the cross section is practically not sensitive to the incident energy. As a result, the pn bremsstrahlung is relatively unimportant as resonance channels become dominant at $E_{kin} \sim 1.5$ GeV.

Bremsstrahlung from pp collisions is expected to be small at low energies due to destructive interferences. However, at the highest energies considered here, the pp bremsstrahlung contribution may be comparable to the pn bremsstrahlung yield [36]. On the other hand, the total contribution of bremsstrahlung is found to be negligible for all practical purposes at those energies (see Sec. III B). Note that the SPA already gives an upper estimate of the expected dilepton yield [37].

III. DILEPTON CROSS SECTIONS IN ELEMENTARY SYSTEMS

Before one can investigate the dilepton production in nucleus-nucleus reactions, one should first check the model

in elementary pp and pd collisions. Recently, the DLS collaboration published a systematic study on dielectron cross sections in light systems for beam kinetic energies E_{kin} from 1 to 5 GeV. The corresponding center-of-mass energies range from below the η production threshold up to 3.6 GeV, where phase space is wide open for the abundant production of a large variety of resonances.

The acceptance of the DLS does not cover the entire phase space. Thus the calculated dilepton pairs are corrected for the limited spectrometer acceptance region. The official DLS-filter V4.1, which has been released for the nucleus-nucleus data only, is applied also for the light systems for which a different filter has been announced. However, the difference between the filters is expected to be negligible for masses above 200 MeV/c [38]. The finite mass resolution of $\Delta M/M \approx 0.1$ is incorporated by folding the calculated spectra, with a Gaussian of width ΔM. The acceptance correction strongly influences the low-mass spectra while the mass resolution smoothing affects the shape of the spectra at higher masses.

A. pp

The resulting dilepton mass spectra for pp collisions are shown in Fig. 4.

Only 0.46 GeV of c.m. energy are available for particle production at $E_{kin} = 1.04$ GeV. Thus, only pion- and Δ-Dalitz decays contribute in this case. The model satisfactorily reproduces the data at low masses, but underestimates them around $M_{e^+e^-} = 0.4$ GeV. The disagreement could be caused by the above-mentioned uncertainties in calculating the electromagnetic form factor of the $\Delta N\gamma$ system. The first generation of DLS data was incompatible to free form factors [3,39]. This situation is now unclear, because the data of the second run tends to exceed the first. However, limited statistics and the better agreement at higher beam energies precludes a definite conclusion on the origin of the "enhancement" at $E_{kin} = 1.04$ GeV.

At $E_{kin} = 1.27 - 1.85$ GeV the model explains the data with growing influence of meson decays. One can see from Fig. 4 that first the η-Dalitz decay and then the direct ρ and ω decay become more important. In the UrQMD calculation of pp, most of the ρ^0 ($\approx 99\%$) are not created in $\pi^+\pi^-$ collisions, but result from heavy baryon decays. The limited phase space at low c.m. energies [22] and the strong (M^{-3}) mass dependence of the dilepton decay widths (14) are responsible for the deformation of the ρ spectrum towards low masses. The cross section for the Dalitz production through Δ decays remains rather constant at low masses, with increasing energy, but increases towards higher masses. Indeed, it is known from $pp \rightarrow n\Delta^{++}$ reactions that heavier Δ's become more important with increasing beam energy due to the mass dependence of the decay widths [40]. In fact, there is a good agreement at intermediate beam energies (disregarding the data point at $M_{e^+e^-} = 200$ MeV) which would be worsened if the electromagnetic $\Delta N\gamma$ form factor would be included, in particular at $E_{kin} \gtrsim 1.6$ GeV.

The model does not reproduce the shape of the measured spectrum at $E_{kin} = 2.1$ GeV and 4.9 GeV. Around $M = 0.6$ GeV the ratio between the pp and pd data decreases for the two highest beam energies. If this gets confirmed, it
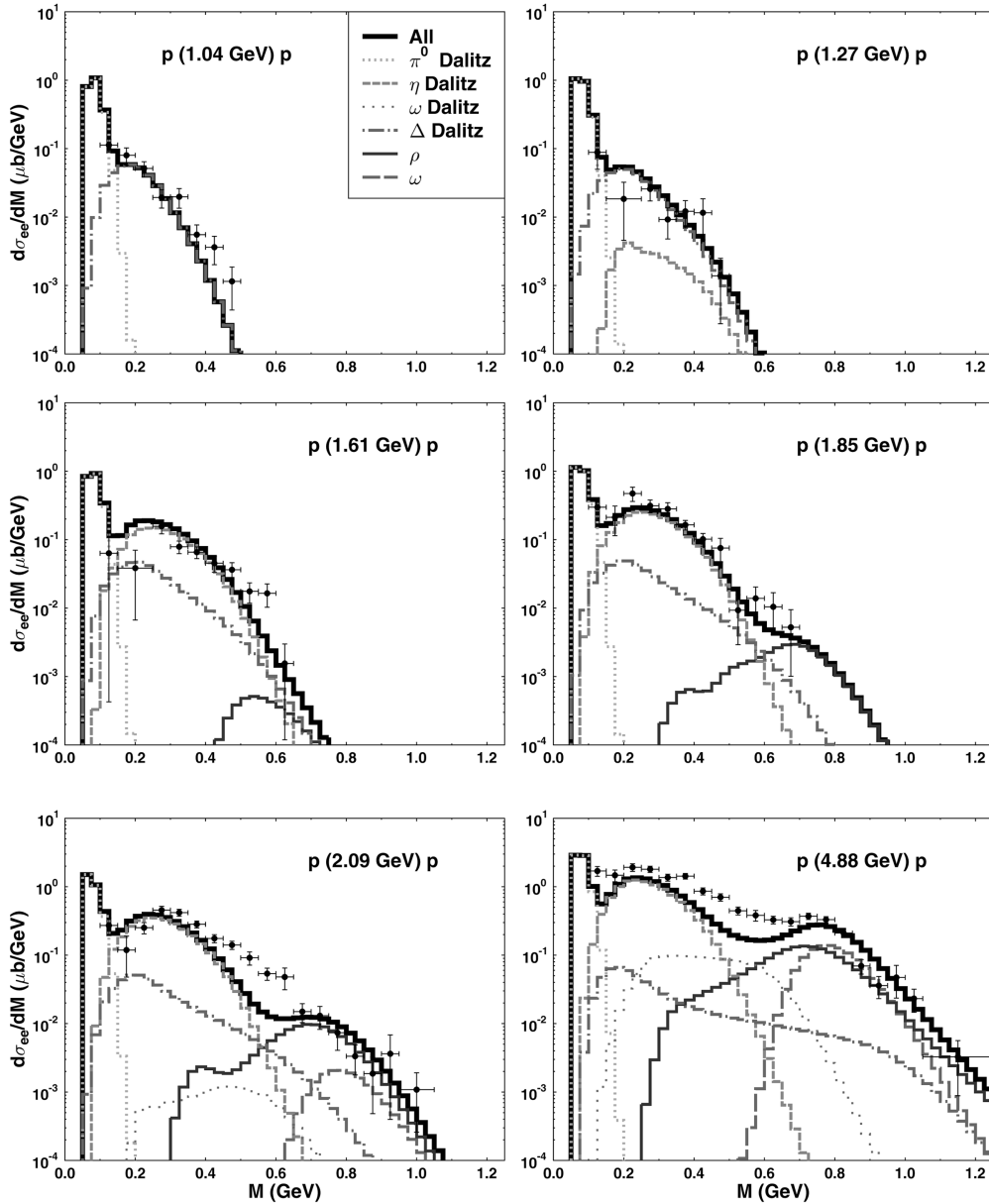
FIG. 4. The e^+e^- mass spectra for pp reactions at six kinetic energies. The upper solid curve is the sum of all contributions. One can see the contributions of π^0 (dotted), Δ (dash-dotted), η (dashed), and ω (dotted) Dalitz decays as well as of the direct ρ^0 (solid) and ω (thin-solid) dilepton decays. Every single dilepton has passed the DLS Filter 4.1 and a mass resolution of 10% is adopted. The data are from [9].

might be explainable by some strong contribution of pp bremsstrahlung, which was not considered here.

B. pd

pd calculations are shown in Fig. 5. The calculated events are minimum-bias triggered at a maximum impact parameter of $b = 1.6$ fm, i.e., a geometric cross section equal to the measured one of about 80 mb.

An important difference to the pp system is due to the internal motion of bound nucleons. This motion smears out the production thresholds. Consequently, one observes subthreshold contributions from η and ρ mesons already at $E_{kin} = 1.04$ GeV.

Unlike in pp collisions, the proton-deuteron data overestimate the model results in the mass region dominated by the

η decay. Note that in the UrQMD model the η production in pn is not modified as compared to pp. This is what one expects from isospin arguments neglecting final-state interactions. However, the pd results indicate an asymmetry in the pp and pn production cross sections as predicted from one-boson exchange models [41]. Indeed, it was measured that just above the threshold, the ratio of pd to pp induced η cross sections is much larger than two [42]. However, due to the Fermi motion in the deuteron, it is not straightforward to extract pn cross sections from pp and pd measurements. On the other hand, direct measurements of the η production in pn are still not available. We have, therefore, evaluated the ratio $R_\eta = \sigma(pd \rightarrow \eta X)/\sigma(pp \rightarrow \eta X)$ without any explicit modification of the pn cross section to estimate the influence of Fermi motion. At $E_{kin} = 1.27$ GeV, close to threshold, we
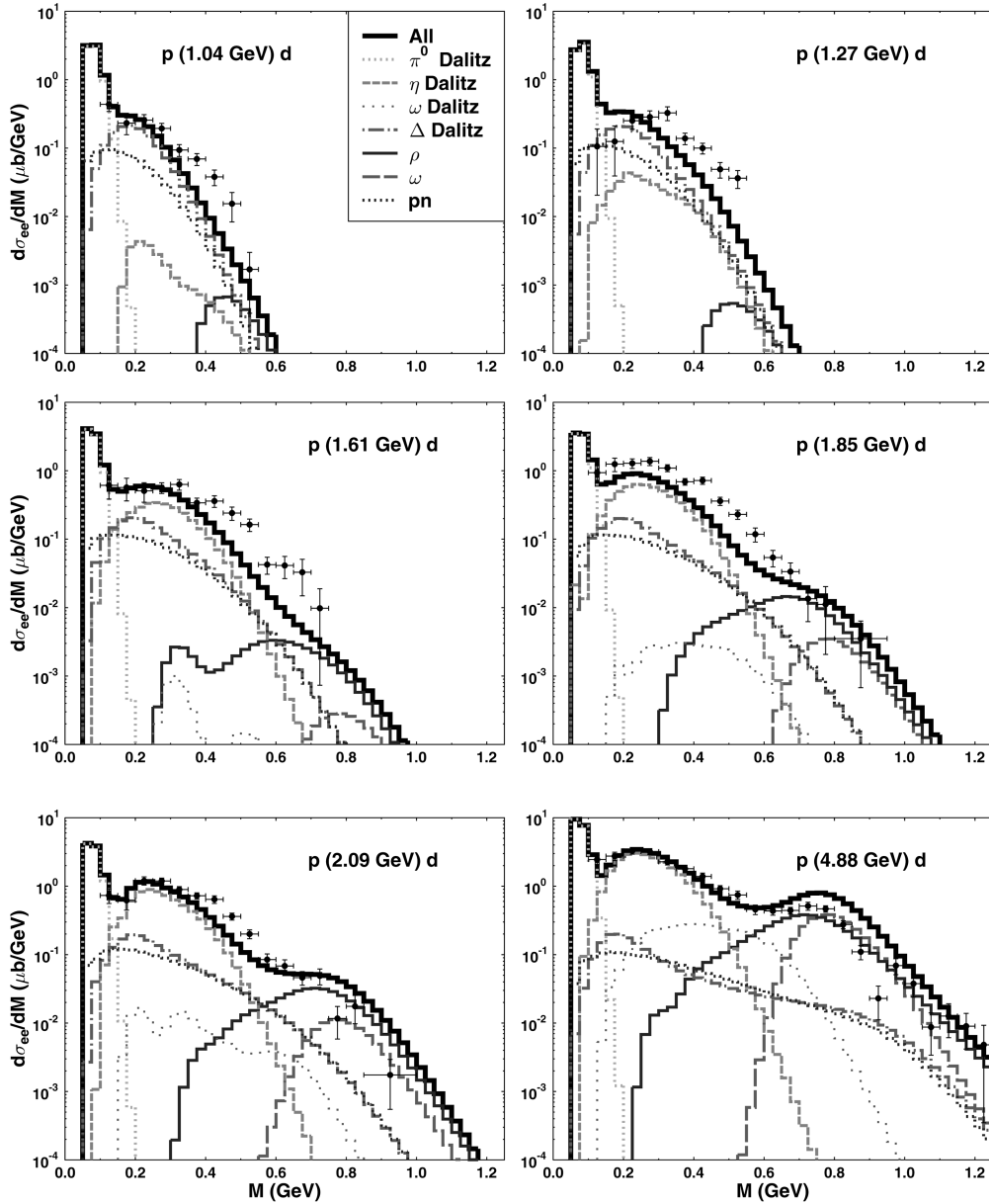
FIG. 5. Acceptance-corrected mass spectra for proton + deuterium. The individual sources are marked as in Fig. 4, but there is an additional contribution from pn bremsstrahlung (thick-dotted).

get the large value $R_\eta = 17 \pm 3$, while above $E_{\text{kin}} = 1.61$ GeV, R_η remains basically constant, between 2.8 and 2.3.

However, the large value of R_η is not enough to explain the integrated total dilepton ratios. This is shown in Fig. 6, where

$$R = \frac{\int_{0.15 \text{ GeV}}^{M_{\text{max}}} \left(\frac{d\sigma_{pd}}{dM} \right) dM}{\int_{0.15 \text{ GeV}}^{M_{\text{max}}} \left(\frac{d\sigma_{pp}}{dM} \right) dM} \qquad (25)$$

is plotted vs the incident energy. The predicted dilepton ratios are rather low at energies smaller than 2 GeV. A similar behavior is also found in BUU calculations [4], which include pp bremsstrahlung. This indicates that there is a com-

mon feature of known transport models with ''conventional'' sources to underestimate the recent DLS nucleus data at intermediate dilepton masses [8]. At $E_{\text{kin}} = 1.27$ GeV the model predicts only $R = 5.2$. This value is lower than the corresponding one of R_η because the η is yet only a marginal dilepton source at this energy.

Within the statistical uncertainties, the mass-differential dilepton cross sections for pd can be explained by the model for the two highest beam energies. Note that pn bremsstrahlung is relatively unimportant.

IV. DILEPTONS IN HEAVY ION COLLISIONS

Figure 7 compares the UrQMD predictions with DLS data for various nucleus-nucleus reactions [8]. At first glance the examined systems all exhibit a qualitatively similar behavior in three distinct mass regions:
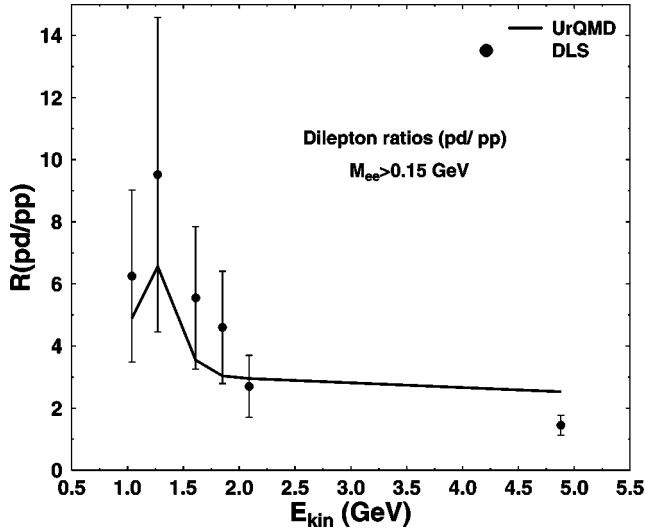
FIG. 6. Ratio of the integrated cross section for pd to pp reactions as a function of the beam energy. The solid line shows the UrQMD result with the DLS filter and resolution. The experimental data are taken from Ref. [9]. Only the larger systematic error bars are displayed.

In the lowest mass region (up to 150 MeV) the spectrum is dominated by the pionic Dalitz decay. There are also strong effects of the acceptance filter, which significantly suppresses the low-mass yield (compare Fig. 2 for the shape of uncorrected Dalitz spectra). Other sources are of little importance in this mass region. However, near $M = 150$ MeV, the Δ Dalitz decay becomes more important.

At intermediate masses the data show a noticeable enhancement of the dilepton yield as compared to the model calculations. There is a considerable confusion about these recent data because the new yields strongly exceed earlier published measurements [43]. The latter have been revised by the DLS collaboration due to large, previously uncorrected, trigger inefficiencies. However, the present calculations and, also, results of other models e.g. [3,44–46], are closer to the earlier measurements in the considered mass range (see Fig. 8).

The theoretical spectrum at $M > 600$ MeV is dominated by direct ρ^0 and ω decays. The model cross sections for dilepton production via ρ mesons nicely account for the data in this region. The two highest data points in He-Ca suffer from lack of statistics. For all nuclear systems, only about 50% of all ρ mesons stem from $\pi^+\pi^-$ annihilations, the other 50% are produced in decays [22].

Turning back to the intermediate region, one sees a similar dilepton enhancement as in the pd data. There one may partially attribute the enhancement to a high $pn \to \eta X$ cross section at the production threshold. Note that our η decay channels in Fig. 7 are lower than in Ref. [46] by about a factor of 2. The same holds in comparison to the analysis of Ref. [47], where the η channel is determined from the measurements of the TAPS Collaboration. These differences might stem from the neglection of the above-mentioned asymmetry of the η production in pp and pn. Inspired by preliminary data of the WASA collaboration, the authors of Ref. [46] use a 6 times larger η production cross section close to threshold for pn than for pp. The fact that UrQMD
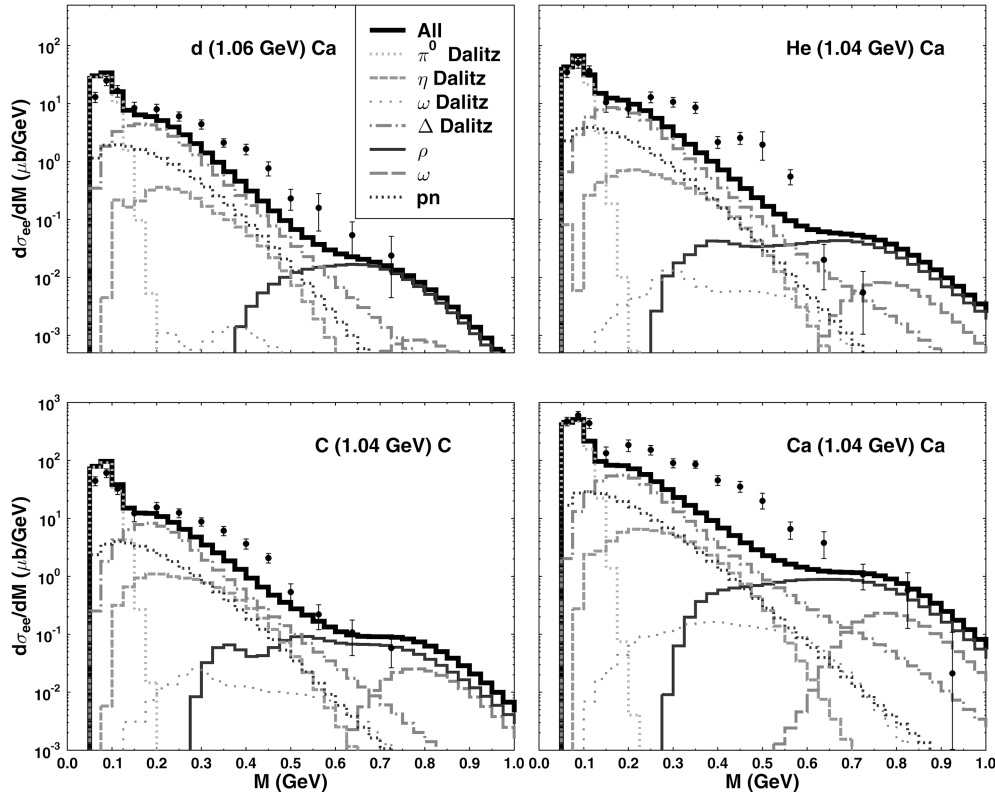

FIG. 7. Model calculations for dilepton spectra from nucleus-nucleus collisions at beam energies of about 1 GeV in comparison to DLS data [8]. The systems $d+$Ca, $\alpha+$Ca, and Ca$+$Ca as well as C$+$C have been examined. See Figs. 4 and 5 for additional information.
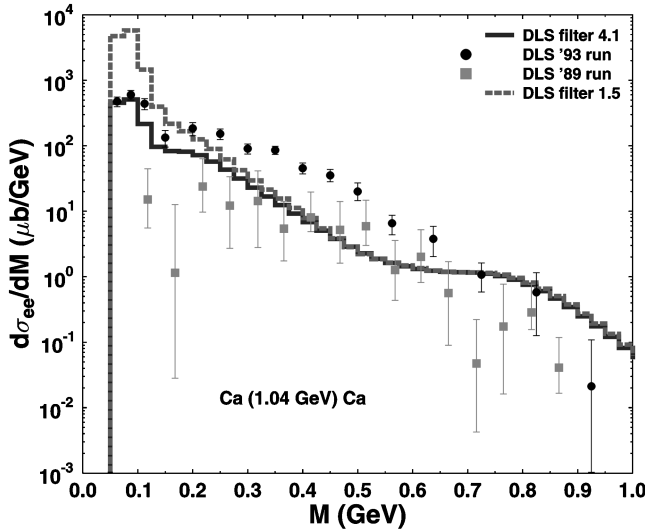
FIG. 8. Total dilepton spectra from Ca+Ca collisions compared to two generations of data. To compare to the earlier measurements [43], the old DLS filter V1.5 (dashed line) has been applied. The solid line corresponds to the calculation of Fig. 7.

FIG. 9. Total dilepton spectra from Ca+Ca collisions with an increased ω width. Also shown are effects due to density dependent modifications of the vector meson masses.

$$m_V^* = m_V(1 - 0.18\varrho/\varrho_0), \tag{26}$$

where $\varrho_{(0)}$ is the local (ground state) density and $m_V^{(*)}$ is the (modified) vector meson mass. Although more sophisticated calculations predict a more complex behavior of the vector meson spectral functions [15], the scaling law seems to be reasonable for the effective masses. To check this idea using the UrQMD model, the poles of the produced quasiparticle vector mesons have been shifted according to Eq. (26) thereby neglecting effects on the vector meson production cross sections. One obtains the dashed curves in Fig. 9. It is found that the dropping mass scenario — and also more complex in-medium spectral functions (see Ref. [46]) — cannot account for the new DLS data.

V. SUMMARY

Dilepton production has been studied within the microscopic nonequilibrium transport model UrQMD. The production mechanisms have been critically revisited. We have compared the model with the DLS data for pp and pd collisions at different beam energies. Resonance decays into dileptons were found to be able to explain the low-energy pp data.

The UrQMD model predictions for the pd system are below the new DLS data for masses 0.3–0.6 GeV. A similar, but even stronger underestimation takes place in collisions of heavier nuclei. The present paper points out that the large enhancement in the data as compared to model calculations cannot be accounted for by two distinct hypotheses on the in-medium modifications of vector mesons. An enhancement of the η production in pn collisions is able to reproduce the yield and shape of the AA spectra. However, huge η production cross sections would be required, in contrast to TAPS data.

overestimates the cross section for $pp \to pp\eta$ (Fig. 1), but underestimates the η production in AA, indicates that threshold effects in the η production are essential and require further investigation.

Therefore, it seems reasonable to reproduce the data by artificially enhancing the η yield. We rescaled the η yield by a factor f_η and found good agreement both in shape and absolute yield with $f_\eta \approx 10$ for C+C and ≈ 20 for Ca+Ca. However, this is not supported by TAPS data which found the 4π extrapolated η cross section in Ca+Ca at 1 GeV to be about 20 mb [48]. Our rescaled cross section corresponds to ≈ 120 mb. A dropping η mass has been introduced in Ref. [46] to explain the DLS data. But these studies also found the increased η cross sections to be incompatible to the TAPS measurements.

We note that the inclusion of a density-dependent $\Delta N\gamma$ form factor for the Δ Dalitz decay, as discussed in Ref. [3], can give a sizable enhancement of the calculated dilepton yield at intermediate masses 0.2 GeV$<M<$0.6 GeV. However, this is ruled out as an explanation, because the fair agreement of the calculation to the data in the high-mass region $M>600$ MeV would be destroyed by a strong overestimation.

Due to σ-ω mixing via an NN^{-1} loop, the 2π decay channel of the ω might be significantly enhanced in nuclear matter [49]. To get an estimate for possible effects on intermediate mass lepton pairs, we have increased $\Gamma_{\omega\to\pi\pi}$ by a factor of 500 to approximately 100 MeV. The solid curves in Fig. 9 show the result of this calculation for the Ca+Ca system. As can be seen, the mass distribution of dilepton pairs from direct ω decays becomes very broad. Nevertheless, this contribution has almost no effect on the total dilepton yield and does not suffice to explain the measured enhancement.

One approach to describe the density dependence of vector meson masses is the linear scaling law of Hatsuda and Lee [50]:
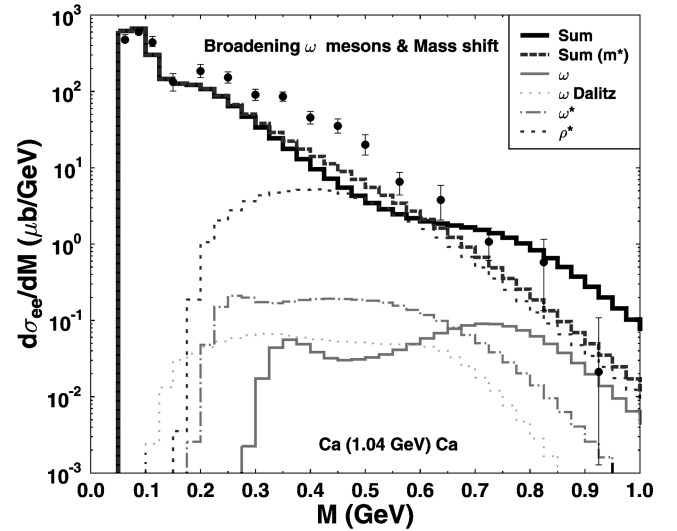
ACKNOWLEDGMENTS

[1] E. L. Feinberg, Nuovo Cimento A **34**, 391 (1976); E. V. Shuryak, Phys. Lett. **78B**, 150 (1978); G. Domokos and J. I. Goldman, Phys. Rev. D **23**, 203 (1981).

[2] C. Gale and J. Kapusta, Nucl. Phys. **A471**, 35c (1987).

[3] G. Wolf *et al.*, Nucl. Phys. **A517**, 615 (1990).

[4] A. I. Titov, B. Kämpfer, and E. L. Bratkovskaya, Phys. Rev. C **51**, 227 (1995).

[5] W. Cassing, W. Ehehalt, and C. M. Ko, Phys. Lett. B **363**, 35 (1995).

[6] C. M. Ko, G. Q. Li, G. E. Brown, and H. Sorge, Nucl. Phys. **A610**, 342c (1996).

[7] E. L. Bratkovskaya and W. Cassing, Nucl. Phys. **A619**, 413 (1997).

[8] R. J. Porter *et al.*, Phys. Rev. Lett. **79**, 1229 (1997).

[9] W. K. Wilson *et al.*, Phys. Rev. C **57**, 1865 (1997).

[10] A. Drees, Nucl. Phys. **A610**, 536c (1996).

[11] J. Stroth, Acta Phys. Pol. B **27**, 3095 (1996).

[12] J. C. Gregory *et al.*, Nucl. Phys. **A566**, 287c (1994).

[13] G. E. Brown and M. Rho, Phys. Rev. Lett. **66**, 2720 (1991).

[14] T. Hatsuda and H. Shiomi, Nucl. Phys. **A590**, 545c (1995).

[15] R. Rapp, G. Chanfray, and J. Wambach, Nucl. Phys. **A617**, 472 (1997); F. Klingl, N. Kaiser, and W. Weise, *ibid.* **A624**, 527 (1997); W. Peters, M. Post, H. Lenske, S. Leupold, and U. Mosel, nucl-th/9708004 1997.

[16] W. Cassing, E. L. Bratkovskaya, R. Rapp, and J. Wambach, nucl-th/9708020, 1997.

[17] J. Aichelin and H. Stöcker, Phys. Lett. B **176**, 14 (1986); H. Sorge, H. Stöcker, and W. Greiner, Ann. Phys. (N.Y.) **192**, 266 (1989); J. Aichelin, Phys. Rep. **202**, 233 (1991).

[18] S. A. Bass, C. Hartnack, H. Stöcker, and W. Greiner, Phys. Rev. C **51**, 3343 (1995).

[19] L. A. Winckelmann *et al.*, Nucl. Phys. **A610**, 116c (1996).

[20] S. A. Bass *et al.*, mcl-th/9803035, Prog. Part. Nucl. Phys., in press.

[21] M. Bleicher *et al.* (unpublished).

[22] L. A. Winckelmann, H. Sorge, H. Stöcker, and W. Greiner, Phys. Rev. C **51**, R9 (1995).

[23] Particle Data Group, R. M. Barnett *et al.*, Phys. Rev. D **54**, 1 (1996).

[24] M. Batinic, I. Slaus, A. Svarc, and B. M. K. Nefkens, Phys. Rev. C **51**, 2310 (1995).

[25] H. Calen *et al.*, Phys. Lett. B **366**, 39 (1996).

[26] J. Murray, W. Bauer, and K. Haglin, hep-ph/9611328, 1996.

[27] N. S. Craigie, Phys. Rep. **47**, 1 (1978).

[28] L. G. Landsberg, Phys. Rep. **128**, 301 (1985).

[29] N. M. Kroll and W. Wada, Phys. Rev. **98**, 1355 (1955).

[30] P. Koch, Z. Phys. C **57**, 283 (1993).

[31] H. F. Jones and M. D. Scadron, Ann. Phys. (N.Y.) **81**, 1 (1973).

[32] A. Hsieh and E. Yehudai, Commun. Phys. **6**, 253 (1992).

[33] U. Heinz and K. S. Lee, Nucl. Phys. **A544**, 503c (1992).

[34] C. Gale and J. Kapusta, Phys. Rev. C **40**, 2397 (1989).

[35] L. A. Winckelmann, H. Stöcker, W. Greiner, and H. Sorge, Phys. Lett. B **298**, 22 (1993).

[36] K. Haglin and C. Gale, Phys. Rev. C **49**, 401 (1994); J. Zhang, R. Tabti, C. Gale, and K. Haglin, Int. J. Mod. Phys. E **6**, 475 (1997).

[37] P. Lichard, Phys. Rev. D **51**, 6017 (1995).

[38] H. Matis (DLS Collaboration) (private communications).

[39] M. Schäfer, H. C. Dönges, A. Engel, and U. Mosel, Nucl. Phys. **A575**, 429 (1991).

[40] V. Dmitriev, O. Sushkov, and C. Gaarde, Nucl. Phys. **A459**, 503 (1986).

[41] T. Vetter, A. Engel, T. Biro, and U. Mosel, Phys. Lett. B **263**, 153 (1991).

[42] E. Chiavassa *et al.*, Phys. Lett. B **337**, 192 (1994).

[43] G. Roche *et al.*, Phys. Lett. B **226**, 228 (1989).

[44] L. Xiong, Z. G. Wu, C. M.Ko, and J. Q. Wu, Nucl. Phys. **A512**, 772 (1990).

[45] E. L. Bratkovskaya, W. Cassing, and U. Mosel, Phys. Lett. B **376**, 12 (1996).

[46] E. L. Bratkovskaya, W. Cassing, R. Rapp, and J. Wambach, nucl-th/9710043, 1997.

[47] R. Holzmann *et al.*, Phys. Rev. C **56**, R2920 (1997).

[48] F. D. Berg *et al.*, Phys. Rev. Lett. **72**, 977 (1994).

[49] G. Wolf, B. Friman, and M. Soyeur, nucl-th/9707055, 1997.

[50] T. Hatsuda and S. H. Lee, Phys. Rev. C **46**, R34 (1992).

[51] V. Flaminio, W. G. Moorhead, D. R. O. Morrison, and N. Rivoire, CERN, Geneva Report No. CERN-HERA-84-01, 1984.